



HAL
open science

Emissivity at high temperature of Ni-based superalloys for the design of solar receivers for future tower power plants

Marianne Balat-Pichelin, Jean-Louis Sans, Eric Bêche, Ludovic Charpentier, Alain Ferrière, Sébastien Chomette

► To cite this version:

Marianne Balat-Pichelin, Jean-Louis Sans, Eric Bêche, Ludovic Charpentier, Alain Ferrière, et al.. Emissivity at high temperature of Ni-based superalloys for the design of solar receivers for future tower power plants. *Solar Energy Materials and Solar Cells*, 2021, 227, pp.111066. 10.1016/j.solmat.2021.111066 . hal-03212943

HAL Id: hal-03212943

<https://hal.science/hal-03212943>

Submitted on 30 Apr 2021

HAL is a multi-disciplinary open access archive for the deposit and dissemination of scientific research documents, whether they are published or not. The documents may come from teaching and research institutions in France or abroad, or from public or private research centers.

L'archive ouverte pluridisciplinaire **HAL**, est destinée au dépôt et à la diffusion de documents scientifiques de niveau recherche, publiés ou non, émanant des établissements d'enseignement et de recherche français ou étrangers, des laboratoires publics ou privés.

Emissivity at high temperature of Ni-based superalloys for the design of solar receivers for future tower power plants

Marianne Balat-Pichelin ^{1*}, Jean-Louis Sans ¹, Eric Bêche ¹, Ludovic Charpentier ¹, Alain Ferrière ¹, Sébastien Chomette ²

¹ Laboratoire PROMES-CNRS, 7 rue du four solaire, 66120 Font-Romeu Odeillo (France)

² Université Grenoble Alpes, CEA, LITEN, 38000 Grenoble Cedex (France)

*Corresponding author: Marianne.balat@promes.cnrs.fr Ph.: +33 4 68 30 77 68

Keywords: Infrared emissivity; high temperature; oxidation; concentrated solar energy; nickel-based alloys; solar receiver

Abstract

In the framework of the H2020 European project POLYPHEM, whose main objective is to improve the flexibility and performance of small-scale solar power plants, studies have been conducted on various nickel-based alloys for the design of the solar receiver. Inconel 600 alloy is used as a reference material in the advanced manufacturing of high temperature solar receivers but other oxidation resistant alloys have been selected such as Inconel 617, Haynes 230, Haynes HR120 and Hastelloy X and the best candidate will be used for making the prototype. Thus, two essential quantities, namely the solar absorptivity α – the higher the better – and the total hemispherical emissivity ε – the lower the better – were measured in high vacuum and under atmospheric air up to 1400 K in the MEDIASE reactor installed at the focus of the 1000 kW solar furnace. The objective is to reach the best solar absorptivity and the α/ε ratio the highest as possible. The emissivity measurement was made by a direct method requiring the measurement of the true temperature of the material using a bi-chromatic pyro-reflectometer and that of its radiance by spectro-radiometry. Total hemispherical emissivity data are presented at the same time as microstructural (SEM, XRD) and topographic (3D profilometry) characterizations allowing the interpretation of the emissivity evolution with temperature and the growth of the oxide layer. Finally, the alloy Haynes 230 was chosen to build the solar receiver.

1. Introduction and context

Solar thermal electricity with integrated thermal energy storage system has demonstrated a high potential to increase the share of renewable electricity in the energy mix. The maximum temperature of liquid heat transfer fluids implemented in Concentrated Solar Power (CSP) plants (830 K) currently limits the solar-to-electric conversion efficiency at about 25%. The development of central solar receivers working at very high temperature (1020 K and more) paves the way to the utilization of engines offering efficiency higher than steam Rankine turbines, like combined cycles or supercritical CO₂ Brayton cycles. The research project POLYPHEM addresses some of the major challenges raised by the development of the next generation of solar tower technologies (Fig. 1). A prototype plant of small-scale solar thermal combined cycle is designed, implemented and operated. The top cycle is a solar-driven micro gas-turbine of 70 kW and the bottom cycle is an Organic Rankine Cycle of 25 kW. A thermal energy storage of 2.6 MWh using thermocline tank is integrated between both cycles.

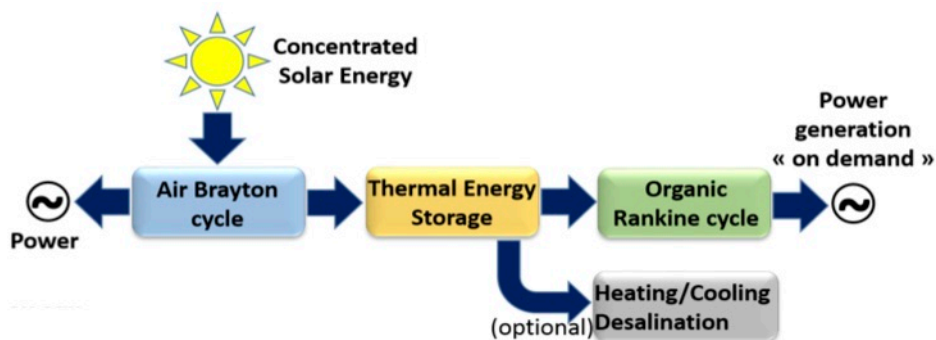


Figure 1. Scheme of the POLYPHEM concept

Conventional fuel is substituted by solar energy in the gas-turbine through the integration of the solar receiver in the air Brayton cycle. The pressurized air solar receiver is a key component, it must be reliable, efficient, cost-competitive and it must offer a long lifetime. Its development addresses material issues, fluid distribution and fluid flow issues, and heat transfer issues. The implementation of metallic materials is preferred. CNRS and CEA have already proposed a new concept of efficient pressurized air solar absorber and have validated it at laboratory scale [1]. The core technology developed is a bundle of thin nickel-based alloy tubes (diameter < 8 mm) arranged in parallel rows and embedded into a highly conductive material (Cu alloy). An external thin plate of nickel-based alloy prevents oxidation

and corrosion of the Cu alloy. Both metallic materials are assembled by diffusion bonding using High Isostatic Pressure (HIP) fabrication process. This process yields no thermal resistance at interfaces. Additional R&D work is necessary to optimize the concept and to adapt it to the specifications of POLYPHEM. The required heat rate is 500 kW under standard solar direct normal irradiance of 1000 W/m². The temperature of the air is increased from 460 K at the inlet up to 1020 K at the outlet, with a maximum allowed pressure drop below 170 hPa (e.g. 5% of the operating pressure of 3320 hPa). The targeted thermal efficiency of the receiver exceeds 80%. The manufacturing cost target will be 0.4 €/W when TRL 9 is achieved.

The material exposed to concentrated solar energy is submitted to strong thermo-mechanical stresses due to temperature gradients increased by the non-uniform solar flux density distribution. The selection of the most reliable alloy for the fabrication of the solar receiver is a critical step of the project. To this end, oxidation resistant metallic alloys were pre-selected. Their optical properties were measured and thermo-mechanical characterizations were also carried out from room temperature up to service representative temperature of the solar receiver.

The literature about oxidation and emissivity at high temperature of Ni-based superalloys is scarce. Main of the studies was carried out in the frame of the development of the Very High Temperature nuclear Reactors (VHTR) [2-8] on Inconel 617, Haynes 230, Hastelloy X and HR 120.

Inconel 617

Oxidation of Inconel 617 was studied up to 1370 K in air by Kim et al. [6] and they have observed a NiO-Cr₂O₃ double-layer that was formed at 1170 K with some isolated triple layer NiO-NiCr₂O₄-Cr₂O₃ structures. At 1370 K, a double layer of inner Cr₂O₃ and outer TiO₂ was formed with some spallation of this last phase.

The normal spectral (3-18 μm) emissivity of Inconel 617 at 570 K was measured by King et al. [2] on non-oxidized samples, and on oxidized ones in a mixture He/H₂O during 500 h at 1300 K. The normal spectral emissivity decreases from 0.20 at 3 μm to 0.10 at 18 μm for the reference non-oxidized sample (Ra = 0.02 μm) and after oxidation with the formation of a thick black layer with an increased roughness (Ra = 1.6 μm), it increases from 0.80 up to a maximum of 0.92 around 13.5 μm and then decreases to 0.30 at 16 and 18 μm.

Haynes 230

About Haynes 230, oxidation at 1170 K and 1370 K has led to the formation of the mixed oxide as for Inconel 617, with an inner layer of Cr_2O_3 and an outer one of MnCr_2O_4 respectively. It was observed that H230 is less oxidized than Inconel 617 and this was attributed to the decreasing diffusion of oxygen through the mixed oxide layer, and for both the alloys the weight change followed a parabolic law [6].

The normal spectral emissivity of H230 measured in the same conditions as for Inconel 617 by King et al. has given nearly the same results with an emissivity going from 0.25 at 3 μm down to 0.10 at 18 μm for the reference non-oxidized sample and after high temperature oxidation during 500 h, the emissivity goes from 0.70 to 0.85 from 3 to 13.5 μm then drops down up to 16 μm , this being correlated to the two absorption bands of Cr_2O_3 between 15 and 18 μm [2]. Another work of Maynard et al. has given some values for the total hemispherical emissivity of H230 [4]. For the as-received non-oxidized sample, the emissivity measured in secondary vacuum (10^{-4} - 10^{-5} Pa) increases from 0.18 around 600 K up to 0.24 around 1400 K, this value being in agreement with the one of Cockeram et al. (0.23 at 1370 K) [9]. After 15 min oxidation in air around 1200 K, the total hemispherical emissivity increases from 0.20 at 600 K up to 0.50 at 1270 K with a sudden increase in the range 1070-1100 K and the main oxide present detected by XRD was NiO.

Hastelloy X

The spectral emissivity of Hastelloy X was measured by Kong et al. [7] and its total hemispherical emissivity by Maynard et al. [3]. Kong et al. measured the normal spectral emissivity in the wavelength range 1-15 μm from 400 to 1200 K on reference and oxidized samples. For the non-oxidized sample, the emissivity decreases from 0.40 down to around 0.20 when the wavelength increases from 1 to 15 μm , according to the electromagnetic theory for metals and increases linearly with the temperature. For the oxidized sample at 1170 K during 720 min, the emissivity is decreasing from 0.80 around 1 μm down to 0.60 at 15 μm with the absorption bands corresponding to the presence of Cr_2O_3 around 11-14 μm . Maynard et al. have measured the emissivity on as-received samples and have obtained values going from 0.18 at 470 K up to 0.28 at 1500 K.

Haynes HR120

We have found only one work on the oxidation of HR120 alloy at 1320 K in air from 30 min up to 100 h [8]. After oxidation, a multi-layered oxide was formed and composed of SiO_2 -

$\text{Cr}_2\text{O}_3\text{-XCr}_2\text{O}_4$ with $X = \text{Mn}$ and/or Fe , Ni from the metal-oxide interface to the top of the oxide scale. For shorter oxidation duration, at 34 min, the oxide layer is only composed of the spinel MnCr_2O_4 and Cr_2O_3 and then after 42 min, the second spinel FeCr_2O_4 grew and this is valid up to 100 h oxidation. No data have been found for the emissivity of the HR120 alloy.

Finally, very few data are available in the literature for non-oxidized Ni-based alloys and for oxidized ones in air at high temperature. The following sections will present the materials and the experimental results obtained for the measurement of emissivity of such alloys to be used as solar receivers in CSP plants.

2. Materials and experimental section

The different alloys selected for the benchmark and the ones of the final selection to be studied are presented. The method for the emissivity determination, the experimental set-up and the experimental protocol are detailed.

2.1. Materials

The solar receiver considered in the European research project POLYPHEM will be manufactured using two types of alloys assembled using diffusion bonding made in a HIP apparatus. The first one is used for the surface in contact with air at high temperature (outer + inner surface of the solar receiver modules and manifolds). The second alloy is used inside the receiver with high thermal conductivity (copper alloy, not studied here). For the first type of material, the selected one needs high temperature oxidation resistance but also high temperature mechanical properties (inside pressure, thermo-mechanical fatigue, creep...). Previous receiver modules were manufactured by diffusion bonding with only nickel-based alloy Inconel 600 parts. However, it was decided to make a material benchmark in the POLYPHEM project in order to find a potential alloy with higher performance as an alternative to alloy Inconel 600. The selection of the benchmark alloys is done thanks to their high temperature oxidation resistance. These alloys are listed in Table 1.

Table 1. List of the superalloys selected for the benchmark

Alloy type	Commercial reference	ISO reference	Major chemical elements
Iron base alloys	800H	1.4876	Fe-Ni-Cr
	330	1.4886	Fe-Ni-Cr
Nickel base alloys	602 CA (6025HT)	2.4633	Ni-Cr-Fe-Al
	690	2.4642	Ni-Cr-Fe
	214	2.4646	Ni-Cr-Al
	617	2.4663	Ni-Cr-Co-Mo
	X	2.4665	Ni-Cr-Fe-Mo
	230	2.4733	Ni-Cr-W-Mo
	600 (ref.)	2.4816	Ni-Cr-Fe
	601	2.4851	Ni-Cr-Fe
	HR-120	2.4854	Ni-Fe-Cr
	HR-160	2.4880	Ni-Co-Cr-Si

The alloy benchmark is principally based on the comparison of the material properties extracted from alloy manufacturer's documentation at 1150 K. This temperature corresponds to the highest one recorded on previous solar receiver modules made by diffusion bonding and tested under solar radiation. The selected physical properties are: high temperature oxidation and nitridation, thermal conductivity and thermal expansion. For mechanical properties, the study focuses on the tensile yield strength at 0.2% offset, tensile elongation to rupture, fatigue, creep strain to obtain 1% of deformation after different duration. The study is completed with an alloy cost comparison based on the supply of plates with a thickness of 5 mm (material manufacturers or retailers alloy cost per kilogram). As the selected material will be used to manufacture a solar receiver, one property has not the same importance as another one. Consequently, the alloys have been classified using a weighting for each property depending on its significance (Figure of Merit). As some properties are not available for all alloys, it was decided to quote to 0 for the corresponding alloy property as no complementary tests are planned to evaluate it. Concerning physical properties, the most important is the high temperature oxidation resistance while the least one is the nitridation resistance. The thermal conductivity and expansion behavior have an average rating as a low thickness of alloy is expected for manufacturing the solar receiver modules. For mechanical properties, the highest weightings have been put on the tensile yield strength and the fatigue response of the alloys. The elongation and the creep behavior (to obtain 1% of deformation after 10000 h) have an average rating, as the expected pressure inside the module is relatively low. Creep properties for reduced time to obtain a

deformation of 1% are not important. A graphic representation of the benchmark results has been made and normalized with the highest score and is reported in Figure 2.

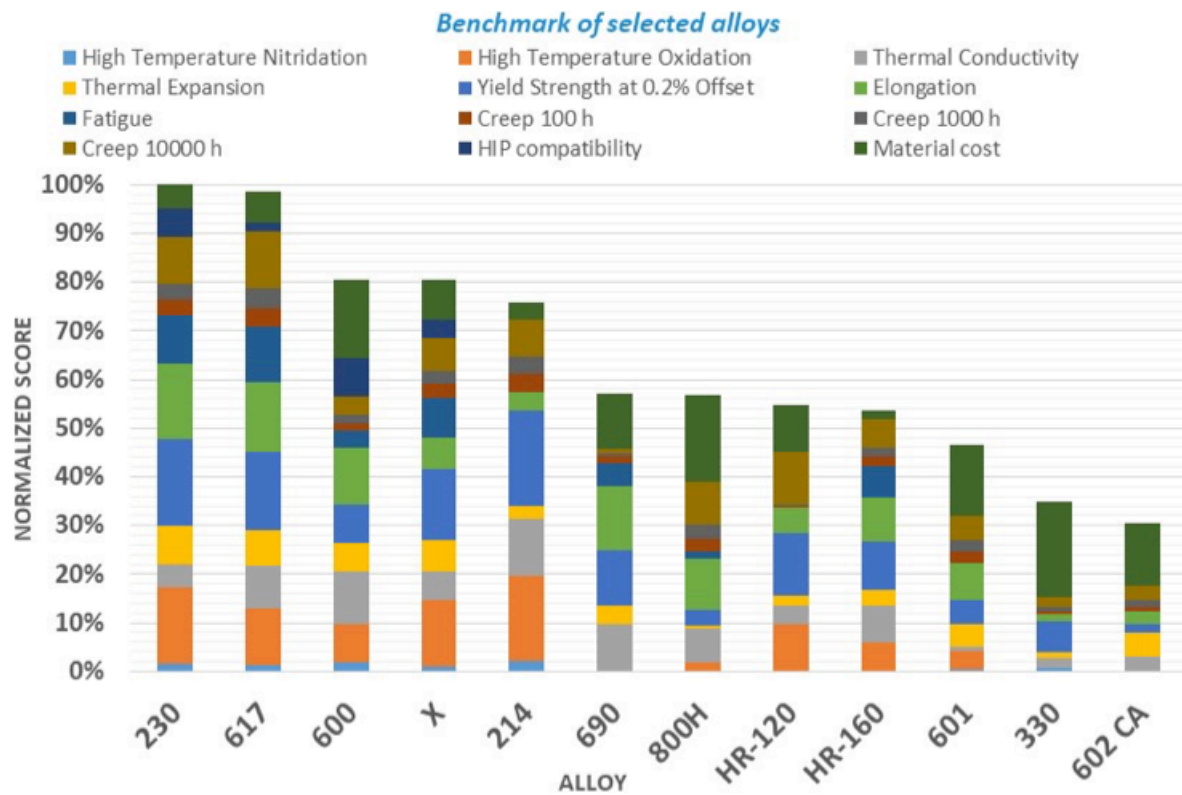


Figure 2. Result of the benchmark of selected alloys

In order to complete the investigations on potential alloys for manufacturing the solar receiver modules, complementary tests are on the four best alloys (manufacturer) of the previous benchmark: Haynes 230 (Haynes), Inconel 617 (Special Metals), Inconel 600 (ThyssenKrupp VDM) and Haynes Hastelloy X (Haynes). The alloy Haynes HR120 (Haynes) has also been tested in order to compare the optical properties of an alloy at the middle of the ranking with the best ones.

2.2. Method for the measurement of the emissivity

The direct method used at PROMES-CNRS laboratory is the one that corresponds directly to the definition of emissivity: the directional spectral radiance (L'_λ) of the material is measured as well as its temperature to calculate the spectral radiance of the blackbody (L^0_λ) at the same temperature [10-12]. The ratio of the radiances gives the spectral directional emissivity:

$$\varepsilon'_\lambda = L'_\lambda / L_\lambda^0$$

The corresponding hemispherical emissivity $\varepsilon_\lambda^\Omega$ is then calculated by integration of the directional values:

$$\varepsilon_\lambda^\Omega = \int_0^{\frac{\pi}{2}} \varepsilon'_\lambda \sin 2\theta \, d\theta$$

The instrument used for radiance measurement is a spectro-radiometer that allows measurements at multiple discrete wavelengths, leading to a finer analysis of the behavior of materials, as for example during oxidation of alloys at high temperature.

The front face of the sample is exposed to the concentrated solar radiation and measurements are made on the rear side of the sample, away from incident solar radiation, in an environment at room temperature. It should be noticed that this causes a temperature gradient in the sample: the insulated face must be brought to a temperature significantly higher than that of the measured face, the thermal gradient depending essentially on the thermal conductivity and the thickness of the sample.

2.3. Experimental set-up

The experimental set-up MEDIASE (Fig. 3) consists of a stainless steel vessel with a capacity of about 60 l, equipped with a turbo-molecular pumping system. A hemispherical silica window, 35 cm in diameter, is placed in front of this vessel and allows concentrated solar radiation to heat the sample (up to 10 MW/m²). The sample (40 mm in diameter, 2 mm thickness) is exposed to concentrated solar radiation by the gradual opening of the doors of the solar furnace. The temperature of the sample is measured on the rear face using the two-color pyro-reflectometer developed at PROMES-CNRS laboratory [13]. This device gives the temperature of the sample without contact with it. Unlike conventional optical pyrometers, this device does not require knowing the emissivity of the sample to obtain its real temperature. To do this, the two-color pyroreflectometer is made up of two parts: one measuring the thermal emission of the sample, the other measuring the bidirectional reflectivities at the two wavelengths. The combination of these two types of measurement allows calculating a common diffusion factor for the two wavelengths that will be used to determine the true temperature of the material. The pyroreflectometer requires two calibrations: one in front of a blackbody (up to 2000 K) equipped with a standard pyrometer,

the other in front of a reflectivity standard to determine the reflectivities of the sample. We obtain a relative uncertainty of the order of 2% on the temperature of the sample.

The radiance measurements are carried out using a spectro-radiometer (CI systems, SR-5000N) equipped with an optic allowing, at the measurement distance used, to observe an area of 9 mm diameter at normal incidence in the center of the sample. The spectral domain studied (0.4-14 μm) does not make it possible to work with a single detector as two systems are present: a spectro-photometer working from 0.4 to 1 μm and a spectro-radiometer operating from 1.3 to 14 μm . We have a blind zone between 1 and 1.3 μm . It produces signals spaced about 30 nm in the range 1.3 to 14 μm and 3 nm in the range 0.4-1 μm , respectively 315 and 1060 wavelengths which is enough to calculate the radiances to the spectral bands chosen.

The measurements are carried out through an original 3-mirrors angular positioner (goniometer) developed at PROMES-CNRS - the sample, the spectro-radiometer and the optical window remaining fixed - at incidence angles from 0° to 80° by 10° step plus 45° and 75° for samples of 40 mm diameter. The nature of the optical window is adapted to the wavelength range studied and in that case it is made of thallium iodo-bromide (KRS5). The spectro-radiometer - goniometer - optical window assembly is calibrated before the series of tests, in front of a blackbody whose temperature is measured with a standard pyrometer.

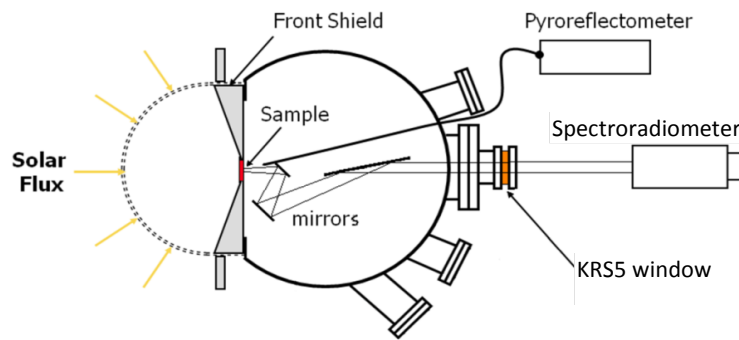
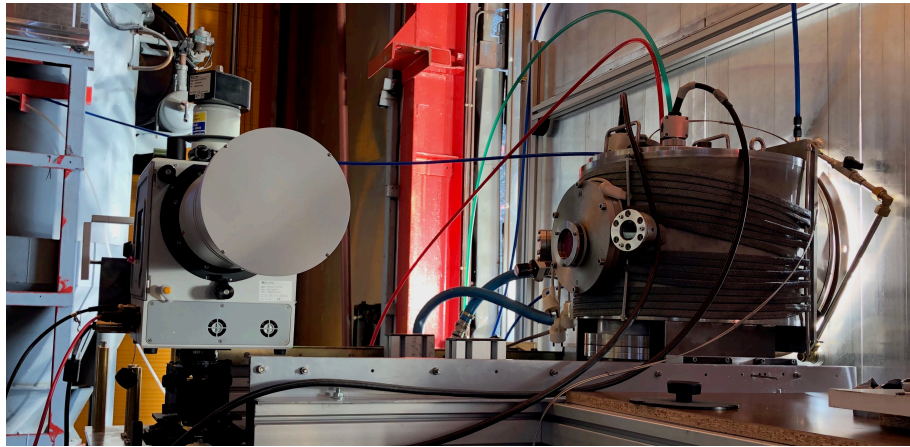


Figure 3. Photo and scheme of the experimental set-up MEDIASE at the focus of the 1000 kW solar furnace in the configuration for emissivity measurement

2.4. Experimental procedure

The samples studied are discs of 40 ± 0.25 mm diameter and 2 to 3 mm thickness. They were delivered by CEA (LITEN / DTBH / SCTR / LCA).

Five alloys (melting temperature) are available: Haynes 230 (1574-1644 K), Haynes HR120 (1573 K), Haynes Hastelloy X (1533-1628 K), Inconel 600 (1627-1686 K) and Inconel 617 (1605-1653 K), 4 discs per grade were received. One as-received sample was kept as reference for surface characterization by SEM, XRD and 3D profilometry.

Measurements were made from 1050 K to 1400 K approximately, in high vacuum and under air at atmospheric pressure, by steps of about 100 K, and for angles of incidence between 0 and 80°. The measured spectral range is between 1.3 and 14 μm .

The sample to be measured is placed in a cooled sample-holder and the chamber is conditioned according to the required measurement conditions. The sample is progressively submitted to concentrated solar radiation until the temperature of the rear face is close to the desired temperature. After adjusting and stabilizing the temperature, the rotation of the goniometer from 0 to 80° is started at the same time as the recording of the spectro-radiometer signal by means of a data acquisition device. Each radiance measurement is preceded and followed by a temperature measurement. The process is repeated at each temperature level. The subsequent data processing consists of:

- extracting the spectro-radiometer signals for each angle of incidence,
- calculating the radiance fractions of the blackbody under the same conditions of temperature and wavelength,
- performing the radiance ratio to calculate the total and/or spectral directional emissivity.

The corresponding hemispherical emissivity is then calculated by integration of the directional values.

3. Experimental results and discussion

The experimental measurement of the radiance up to 1400 K, in the two interested wavelength ranges 1.3-2.8 μm - approximating the solar absorptivity - and 1.3-14 μm for the total emissivity, for the five alloys studied was carried out and the data are reported in the following sections according to the atmosphere surrounding the samples.

a) In high vacuum

The emissivity in high vacuum up to 1300 K was measured for all the alloys to have a reference data for non-oxidized materials. Figure 4 presents the results and Table 2 gives the coefficients a and b of the linear regression: $\varepsilon = a.T + b$.

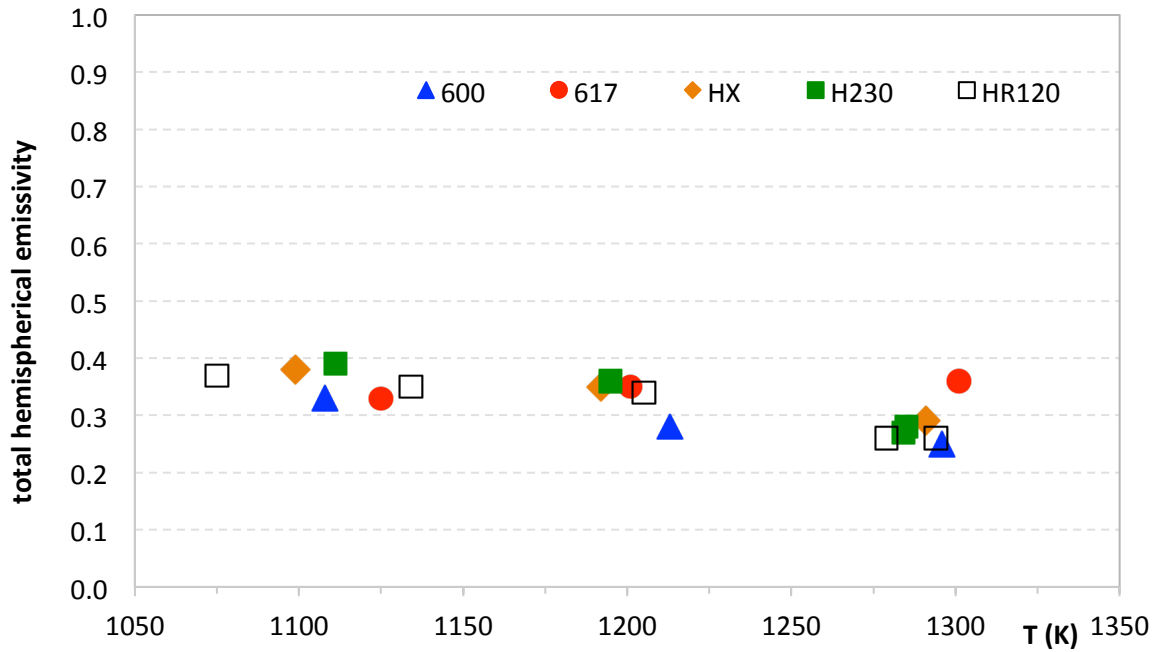


Figure 4. Total hemispherical emissivity versus temperature for the five alloys studied in high vacuum

Table 2. Parameters for the linear regression of emissivity versus temperature

Alloy	Total pressure (Pa)	Coefficient a	Coefficient b	R ²
600	1.5×10^{-3}	-4×10^{-4}	0.8024	0.9943
617	2.3×10^{-3}	2×10^{-4}	0.1450	0.9295
HX	2.5×10^{-3}	-5×10^{-4}	0.9014	0.9707
H230	2.4×10^{-3}	-7×10^{-4}	1.1682	0.9492
HR120	2.0×10^{-3}	-5×10^{-4}	0.9501	0.9002

When the alloys are compared, the results show that except the data for the 617 at 1300 K, the alloys follow nearly the same trend concerning the total hemispherical emissivity versus temperature with a slight decrease when the temperature increases (Fig. 4). The emissivity goes almost from 0.35-0.40 around 1100 K down to 0.25 at 1300 K. Only the alloy 617 still keeps a constant behavior with a total emissivity comprised between 0.30 and 0.35.

In fact, the emissivity decreases when the temperature increases due to the smoothing of the surface at high temperature, this being in relation with the coarsening of the grains. This phenomenon can be observed when looking at the surface morphology of the samples acquired by SEM (Fig. 5) and surface roughness measured by 3D profilometry and reported in Table 3. For all the alloys except for 617, the mean square surface roughness Sq decreases

when the temperature increases. Once again, alloy 617 does not show the same trend as the surface roughness increases when exposed to high temperature going from $Sq = 1.33 \pm 0.03 \mu\text{m}$ for as received samples up to $Sq = 1.47 \pm 0.07 \mu\text{m}$ for the sample heated up to 1300 K.

Table 3. Surface roughness of the alloys before (as received) and after exposure in high vacuum up to 1300 K (S_a arithmetic and S_q mean square surface roughness)

Alloy	600	617	H230	HX	HR120
	ref / after				
S_a (μm)	0.98 / 0.85	1.00 / 1.12	0.76 / 0.66	0.85 / 0.82	0.91 / 0.84
S_q (μm)	1.29 / 1.16	1.33 / 1.47	1.02 / 0.91	1.19 / 1.13	1.22 / 1.15

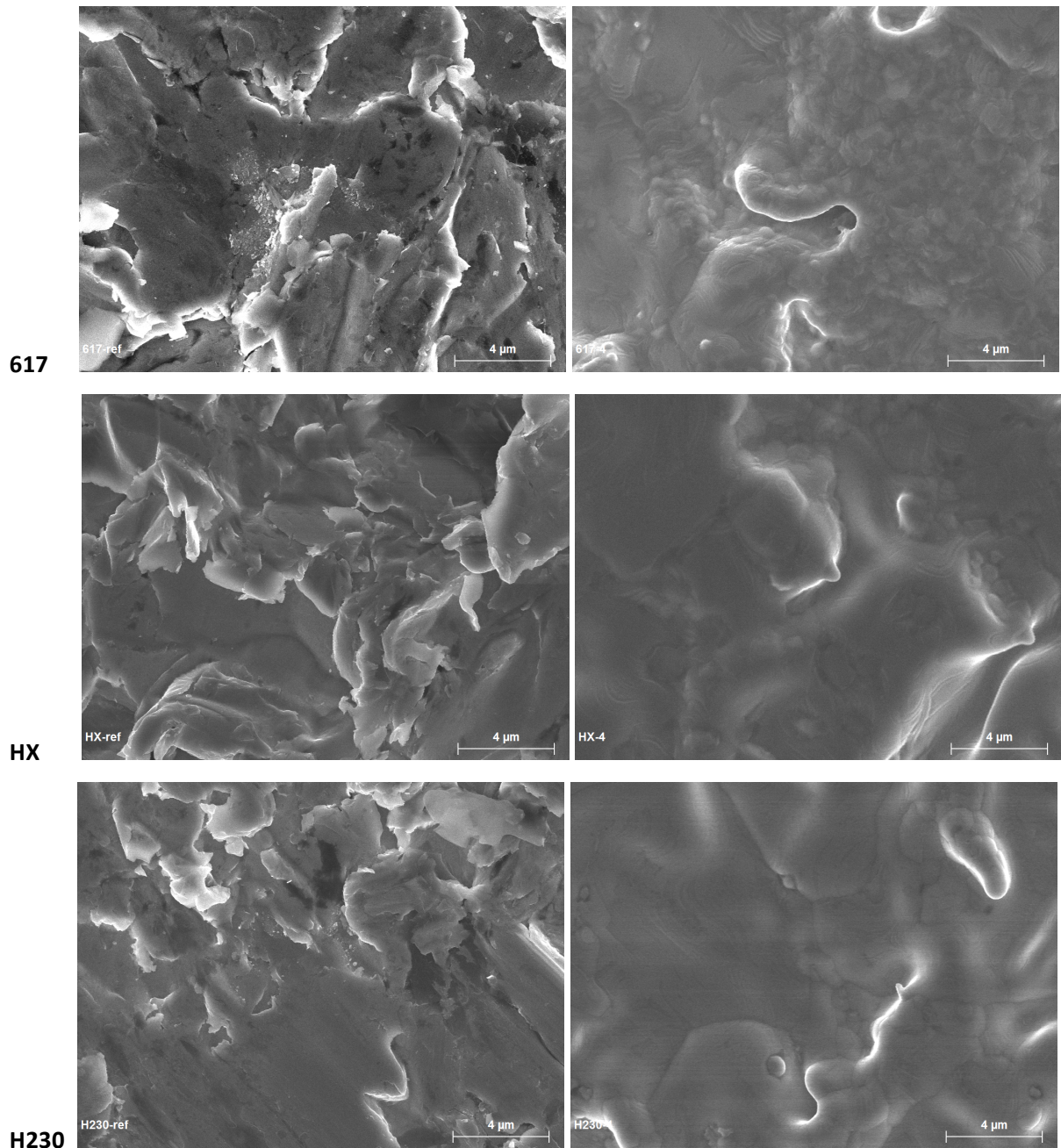


Figure 5. SEM micrographs of the three alloys studied, on the left column, as-received samples and on the right column, after exposure in high vacuum up to 1300 K

XRD characterization was carried out on the samples before and after heat treatment in high vacuum and an example of XRD pattern is given for alloys HX and H230 in Figure 6. One crystalline phase was identified. The diffraction peaks observed for heated samples revealed higher peak intensities and thinner peak FWHM in comparison with the diffractograms collected for the as-received reference samples. This result indicates a higher crystallinity of the heated sample in vacuum. A decreasing of the volume of the lattice is also observed. No

metal or alloy oxide was detected for the heated samples (1300 K) in vacuum.

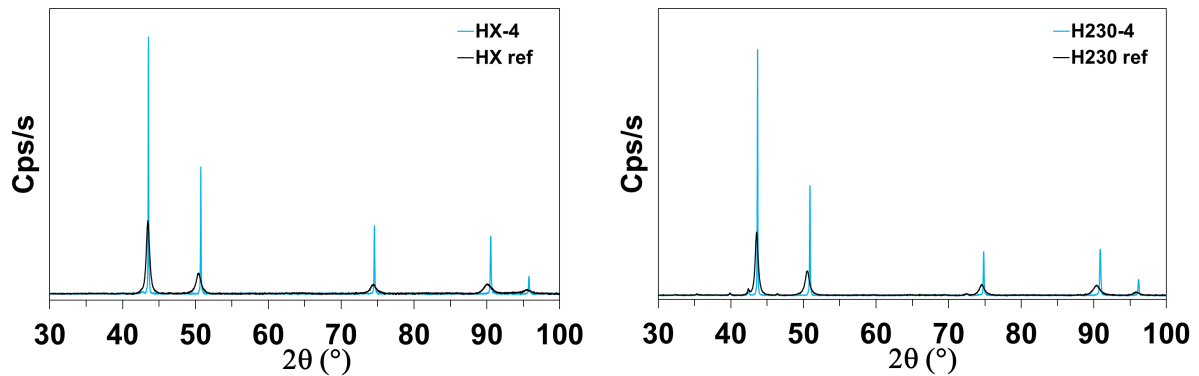


Figure 6. Diffraction patterns of samples HX and H230 before (ref) and after heat treatment in high vacuum at T max = 1300 K

b) At atmospheric pressure

Concerning the measurement of the directional emissivity during in situ oxidation, the example of results obtained for the alloy HR120, shown in Figure 7, prove that between angles of incidence of 0° and 60°, no difference can be observed whatever the wavelength in the studied range (1.3-14 μm). For higher angles, the emissivity decreases when the angle increases. Another result is that oxidation increases the emissivity for long wavelengths in the infrared domain (same samples tested at different temperature levels).

It can be noticed that for such oxidized sample, no oscillation of the spectral emissivity can be visible for the short wavelengths as the oxide layer is too thick and opaque to see this effect. This is confirmed later by the SEM images presented in Figure 9 and the XRD patterns in Figure 10.

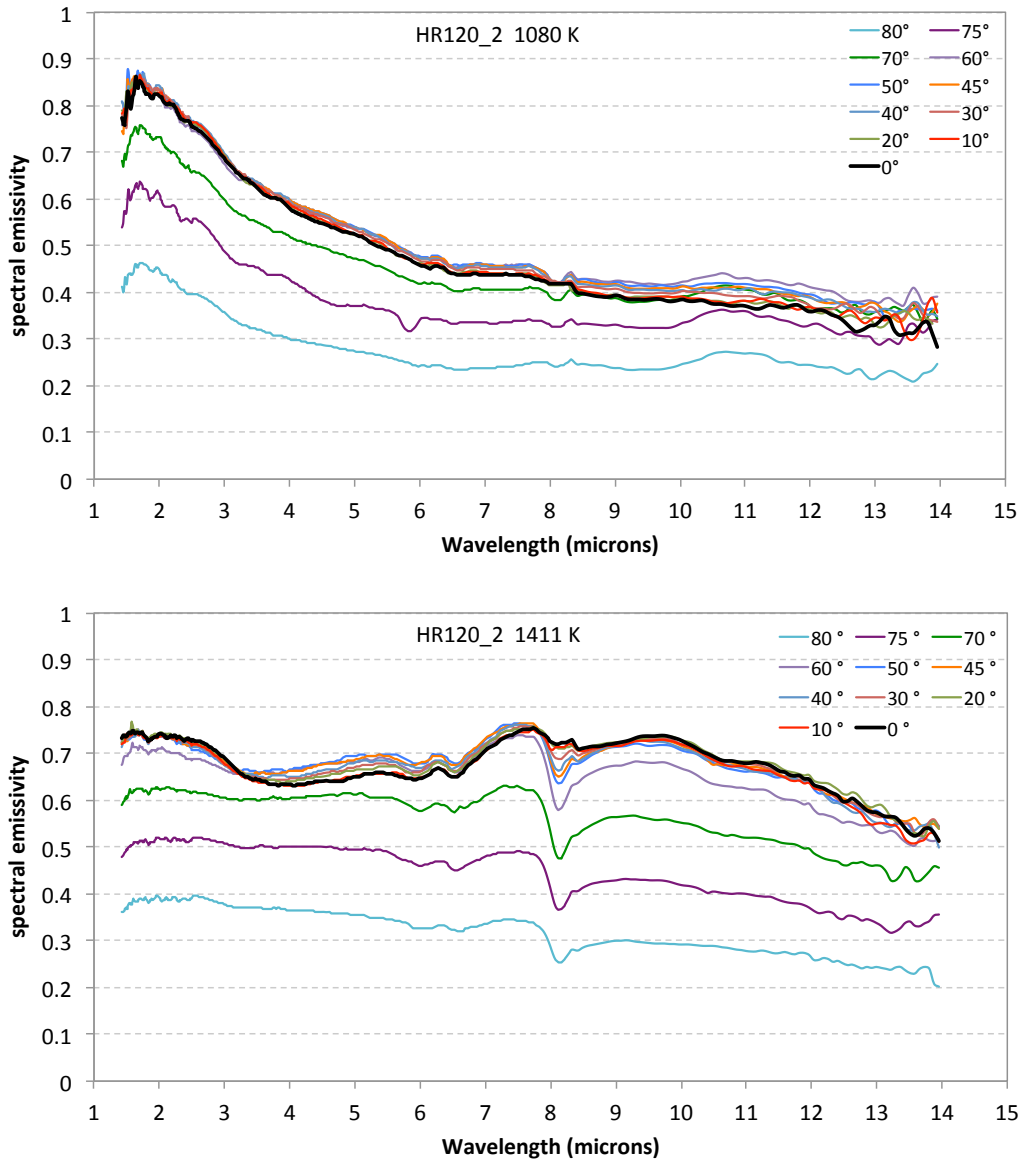


Figure 7. Directional emissivity versus wavelength during in situ oxidation – Example of alloy HR120 at 1080 K (up) and 1410 K (down)

From the directional measurement shown in Fig. 7, we can obtain by integration the hemispherical emissivity in the two wavelength ranges: 1.3-2.8 μm approximating the solar absorptivity and 1.3-14 μm for the total emissivity. The measurement was performed up to 1200 K for one sample of each alloy and up to 1400 K for another one. Figure 8 reports the results obtained for the five alloys, and Table 4 gives the parameters obtained for the linear regression of the total hemispherical emissivity: $\varepsilon = a.T + b$.

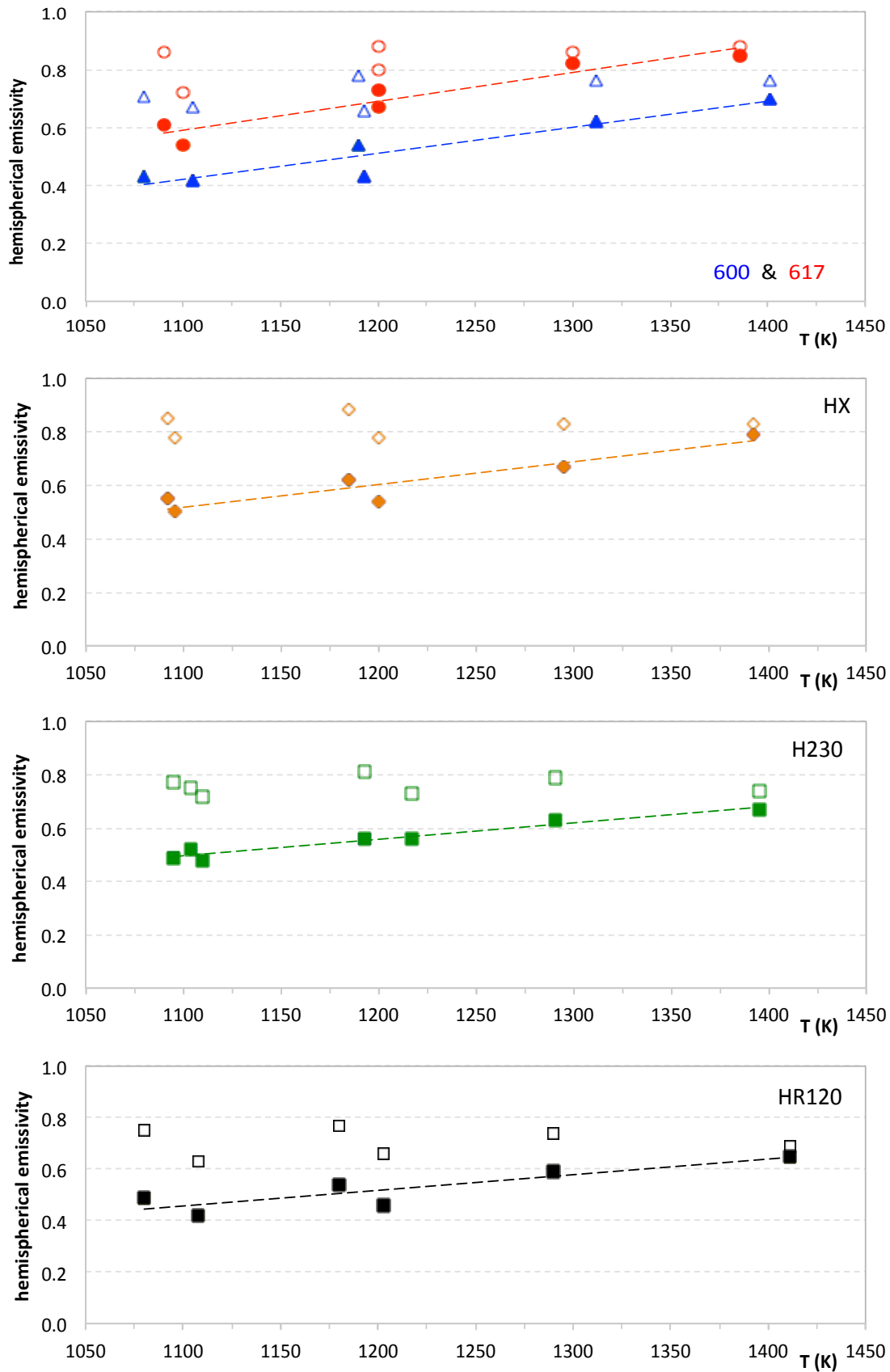


Figure 8. Hemispherical emissivity versus temperature during in situ oxidation of the several alloys up to 1400 K (plain dots for total hemispherical emissivity and open dots for solar absorptivity; triangles for alloy 600 and dots for alloy 617 in the upper graph)

Table 4. Parameters for the linear regression for the total hemispherical emissivity

Alloys	Coefficient a	Coefficient b	R ²
600	9×10^{-4}	- 0.5681	0.8852
617	10^{-3}	- 0.5059	0.9036
HX	9×10^{-4}	- 0.4192	0.8707
H230	6×10^{-4}	- 0.1815	0.9532
HR120	6×10^{-4}	- 0.2114	0.7579

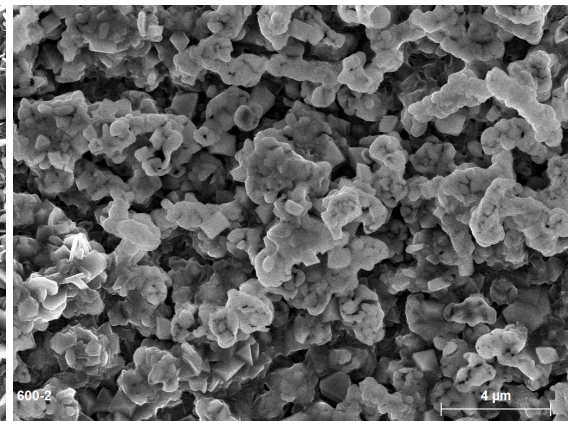
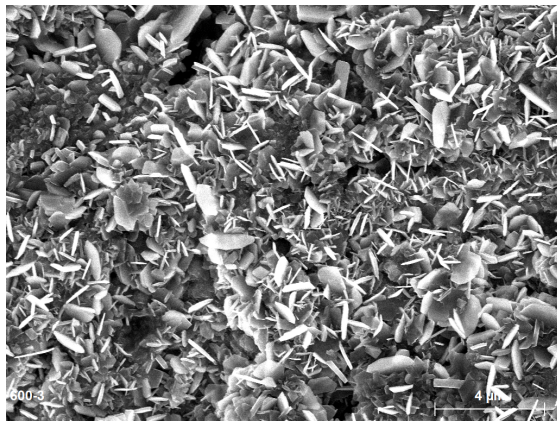
Looking at Figure 8, it clearly appears that the total hemispherical emissivity is increasing with temperature and this is due to the formation of oxide compounds on the surface as already observed for other metallic materials [14, 15]. On the contrary, the approximated solar absorptivity is quite stable in the temperature range 1100-1400 K.

When the total hemispherical emissivity in the wavelength range 1.3-14 μm and the solar absorptivity in the wavelength range 1.3-2.8 μm for alloys 600, HX, H230 and HR120 are compared at different temperatures, some differences can be observed with a higher emissivity and absorptivity for alloy HX than for the others, for example. However, the comparison of the α/ϵ ratio shows no real differences, sign of similar behavior for these alloys (Tables 5).

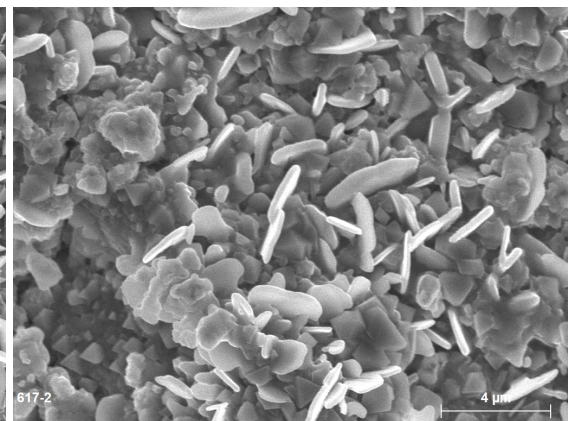
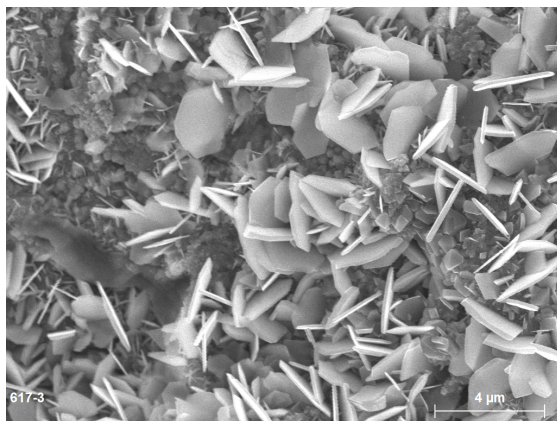
Table 5. Ratio of the solar absorptivity to the total emissivity α/ϵ for four temperature levels

T (K)	600	617	H230	HX	HR120
1100	1.63	1.37	1.53	1.55	1.52
1200	1.48	1.20	1.30	1.43	1.43
1300	1.23	1.05	1.25	1.24	1.25
1400	1.09	1.04	1.10	1.05	1.06

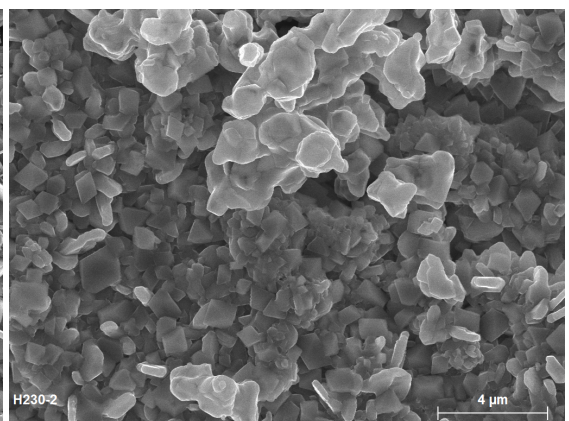
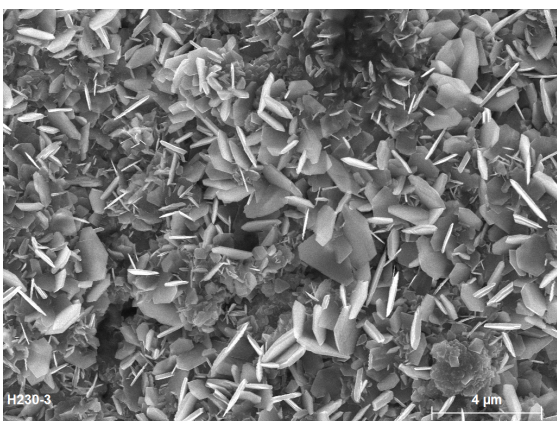
600



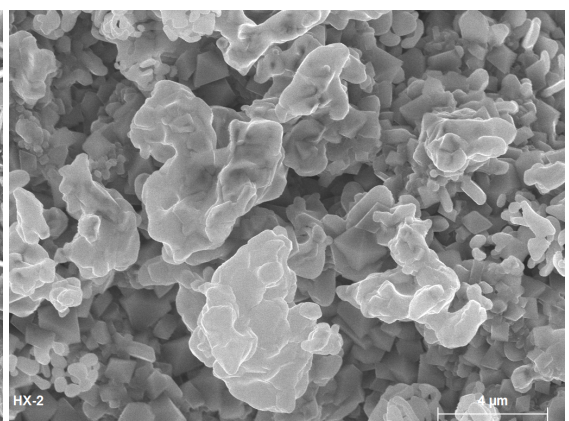
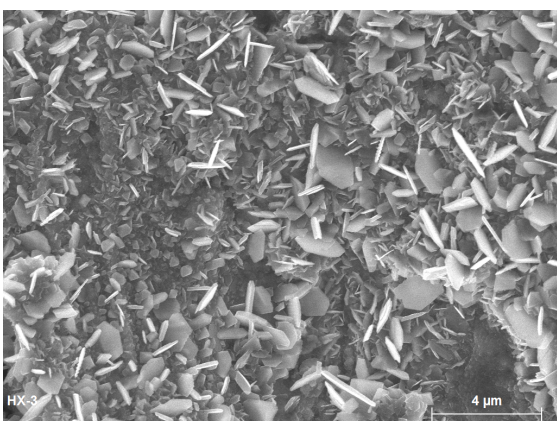
617



H230



HX



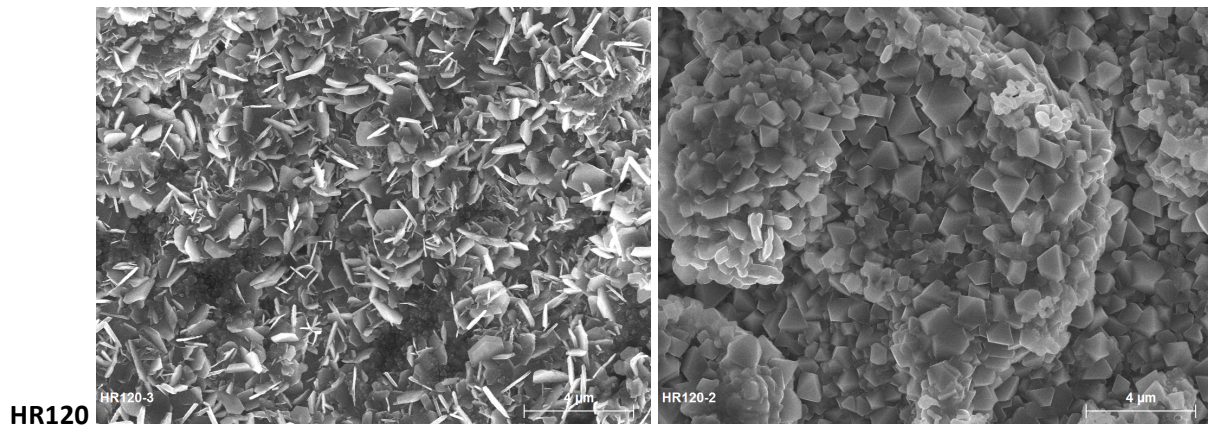


Figure 9. SEM images for the five alloys showing the evolution of the oxidized surfaces after high temperature exposure in air (on the left column, after exposure at 1200 K and on the right column after 1400 K)

In the same way, the SEM images of the surfaces of the alloys 600, HX, H230 and HR120 after oxidation up to 1200 K do not show significant differences, but some differences can be observed up to 1400 K even if the grain size is close (Fig. 9). In all cases, the oxidized surface is full of small and numerous thin flat grains for heat treatment up to 1200 K. This surface morphology evolves to bigger shape oxides at 1400 K. Only the grain size varies from one alloy to another. The behavior of the alloy 617 is slightly different compared to the one of other materials. Indeed, Figure 8 shows that the calculated solar absorptivity is above the level obtained for other alloys (close to 0.90 when others are near or lower than 0.80). However, the total hemispherical emissivity is very high too. That is why the α/ϵ ratio is reduced for alloy 617 from 1100 to 1300 K compared to the other materials but similar at 1400 K (Table 5). Observing the oxidized surface of alloy 617 samples, the thin flat grains formed during oxidation in air up to 1200 K for all previous alloys are also visible on the 617 samples (image on the left, Fig. 9). Nevertheless, while these tips disappeared for oxidation up to 1400 K on previous materials, they are still present on the surface of the 617 samples (image on the right, Fig. 9). The different behavior of the alloy 617 compared to all the other materials could be explained by the fact that the 617 samples were machined in a bar while all the others come from plates. The thermo-mechanical treatments are different for bars and for plates during the manufacturing process that can lead to different initial microstructure and internal stress. Moreover, the surface roughness of the as-received 617 sample is higher than the one for the other alloys (Table 3).

Table 6 gives the results obtained for the surface roughness measurement carried out on the oxidized surface after heat treatment at 1400 K.

Table 6. Surface roughness of the alloys after exposure up to 1200 and 1400 K (Sa arithmetic and Sq mean square surface roughness)

Alloy	600	617	H230	HX	HR120
	1200 K / 1400 K				
Sa (μm)	1.39 / 1.38	1.46 / 1.53	1.30 / 1.36	1.44 / 1.52	1.24 / 1.33
Sq (μm)	1.71 / 1.70	1.83 / 1.90	1.57 / 1.69	1.81 / 1.93	1.56 / 1.67

Looking at the results presented in Table 6, increasing the temperature leads to an increase of the oxidation layer that induces a slight increase of the surface roughness of the samples, except for the alloy 600. The increase of the surface roughness with temperature has an important effect on the emissivity as emissivity is always increasing with the roughness [3, 11, 12, 14-16].

XRD analysis was carried out to identify the oxide compounds present on the surface after oxidation (2θ from 20° to 100°). A part of the XRD patterns (zoom in the range 20° to 45°) is presented in Figure 10 for all the samples studied after heat treatment at 1200 and 1400 K.

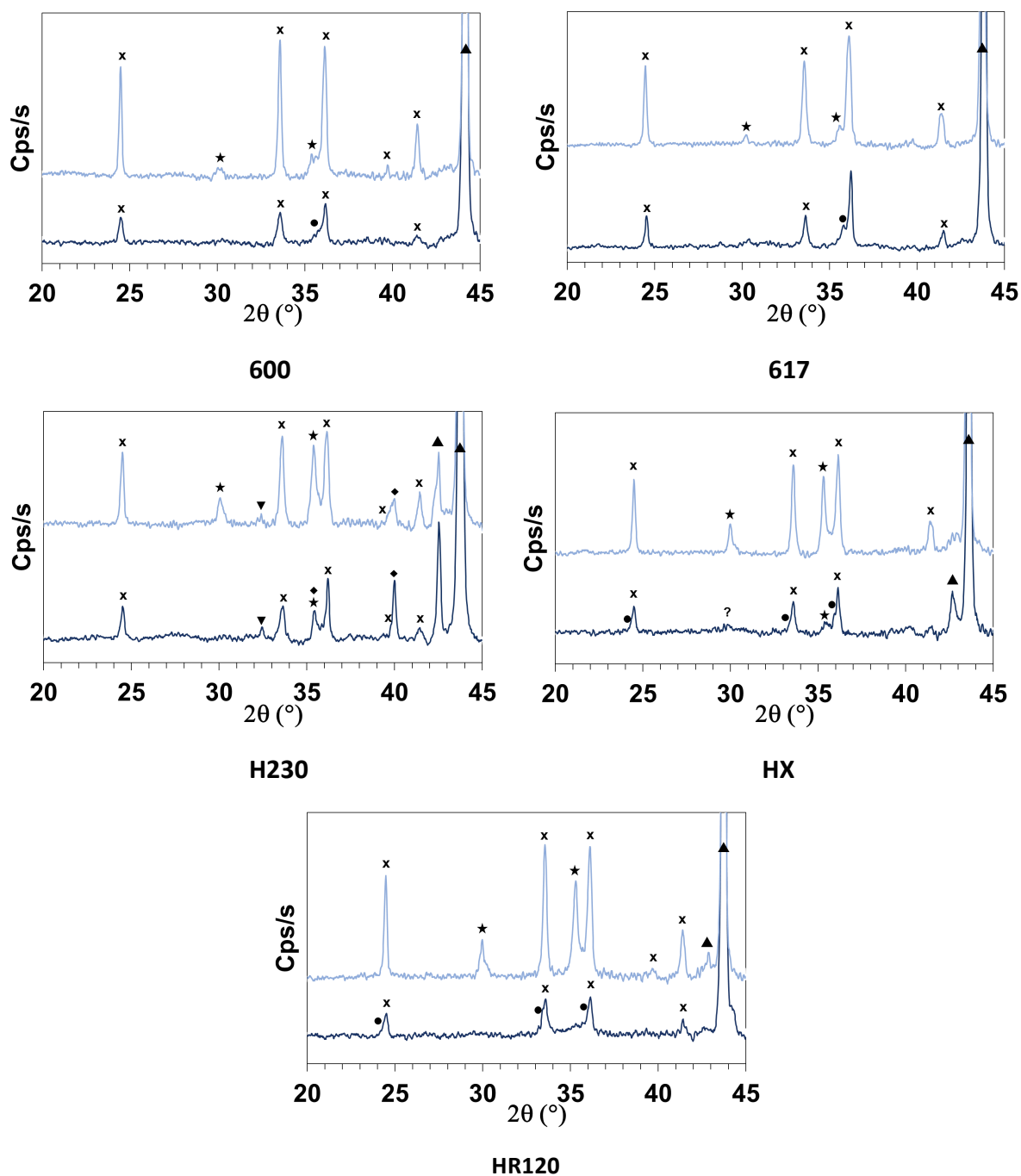


Figure 10. Smoothed diffraction patterns (20° - 45°) collected for heated samples in air (high: at 1400 K, low: at 1200 K). The symbols are associated to the following species: black triangle with tip up: alloy; cross: Cr₂O₃; full dot: Fe₂O₃; star: Fe_{2.93}O₄ or Fe₃O₄; black triangle with tip down: MoO₃; black diamond: W₃O

For the alloys 600 and 617, three metal oxide crystalline phases were identified: chromium (III) oxide, Cr₂O₃ (ICDD 73-6214), iron oxide, magnetite Fe₃O₄ (ICDD 89-0688) and iron (III)

oxide, hematite, $\alpha\text{-Fe}_2\text{O}_3$ (ICDD 84-0311). Higher is the temperature, higher is the amount of Cr_2O_3 (and Fe_3O_4) compounds. The Fe_3O_4 crystalline phase was only detected for the sample heated at 1400 K. A minor Fe_2O_3 phase was observed for the sample heated at 1200 K. Higher is the temperature, higher is the thickness of the oxide layer, the metal oxides being mainly composed of Cr_2O_3 compound.

For the alloy H230, four metal oxide phases were identified: a majority of Cr_2O_3 and Fe_3O_4 , molybdenum oxide Mo_3O (ICDD 065-4549) and tungsten oxide W_3O (ICDD 73-2526). The Fe_3O_4 crystalline phase was mainly detected for the sample heated at 1400 K. For the sample heated at 1200 K, Fe_3O_4 (oriented 311, $2\theta = 35.38^\circ$) is not detected because the diffraction peak located at about 30.05° (220) is missing. The feature located at 35.38° also contains the contribution of the W_3O diffraction peak (about 20 %). Fe_2O_3 was not clearly observed for the sample heated at 1200 K but two other metal oxide phases, W_3O and Mo_3O , were mainly detected at 1200 K.

For HX alloy, as for the alloys 600 and 617, three main metal oxides were detected: Cr_2O_3 , $\text{Fe}_{2.93}\text{O}_4$ (ICDD 86-1353) and Fe_2O_3 . Again, higher is the temperature, higher is the amount of Cr_2O_3 , lower is the amount of Fe_2O_3 that was not detected for the sample heated at 1400 K. The $\text{Fe}_{2.936}\text{O}_4$ crystalline phase was only detected for the sample heated at 1400 K. Again, higher is the temperature, higher is the thickness of the oxide layers, the metal oxides being composed of Cr_2O_3 and $\text{Fe}_{2.936}\text{O}_4$ compounds.

Finally, for the HR120 alloy, three main metal oxides were detected: Cr_2O_3 , Fe_2O_3 and less $\text{Fe}_{2.93}\text{O}_4$. Again, higher is the temperature, higher is the amount of Cr_2O_3 , lower is the amount of Fe_2O_3 not detected for the sample heated at 1400 K. The $\text{Fe}_{2.936}\text{O}_4$ crystalline phase was only detected for sample heated at 1400 K. Higher is the temperature, higher is the thickness of the oxide layers visible by the decreasing intensity of the alloy peak and the increasing one of the peak of the metal oxides composed of Cr_2O_3 and $\text{Fe}_{2.936}\text{O}_4$ compounds. Table 7 reports the main oxides present on the surface of the different alloys. Clearly, the chromium oxide is the main one formed and on all the samples, no NiO nor mixed oxides was detected in agreement with the results of Marchetti et al. [5], King et al. [2] and Kong et al. [7], and on the contrary to the results of Maynard et al. [4] and Kim et al. [6].

Table 7. Main oxide compounds present on the surface of the different alloys treated up to 1400 K

Alloys	Main Crystalline phases
HX	$\text{Cr}_2\text{O}_3 + \text{Fe}_{2.936}\text{O}_4$
H120	$\text{Cr}_2\text{O}_3 (+ \text{Fe}_2\text{O}_3 \text{ or } \text{Fe}_{2.936}\text{O}_4)$
H230	$\text{Cr}_2\text{O}_3 (+ \text{Fe}_2\text{O}_3 - \text{Fe}_3\text{O}_4)$
600	Cr_2O_3
617	Cr_2O_3

4. Conclusion

The benchmark concerning the potential alloy used for manufacturing the solar receiver module part in contact with high temperature air leads to the characterization of five superalloys and the final selection of the nickel-based alloy H230. However, the reference alloy 600 employed for making previous solar receiver is also well ranked. Optical properties evaluation in real conditions does not change the results.

The optical measurements carried out at high temperature on alloys 600, HX, H230 and HR120 samples show low differences in emissivity and solar absorptivity. Only alloy 617 properties are different (worse performance) that could be explained by the oxide morphology but also by the alloy supply (from a rod and not from a plate compared to the others). The evolution of the emissivity with temperature was explained through the characterization of the material surface using SEM, XRD and 3D profilometry, and linear laws were obtained for the total hemispherical emissivity up to 1300 K in high vacuum and up to 1400 K in air at atmospheric pressure, the solar absorptivity being quite constant in the same temperature range.

Acknowledgments

The Polyphem project has received funding from the European Union's Horizon 2020 research and innovation programme under grant agreement n° 764048.

The authors want to also thank the programme "Investissements d'Avenir" (Investment for the Future) of the Agence Nationale de la Recherche (National Agency for Research) of the French State under award number ANR-10-EQPX-49-SOCRATE.

References

- [1] D. Bellard, A. Ferrière, F. Pra, R. Couturier, Experimental characterization of a high temperature pressurized air solar absorber for the PEGASE project, Proc. 18th SolarPACES International Conference, Marrakech (Morocco), september 2012.
- [2] J.L. King, H. Jo, A. Shahsafi, K. Blomstrand, K. Sridharan, M.A. Kats, Impact of corrosion on the emissivity of advanced reactor structural alloys, *J. Nucl. Mat.* 508 (2018) 465-471.
- [3] R.K. Maynard, T.K. Ghosh, R.V. Tompson, D.S. Viswanath, S.K. Loyalka, Total hemispherical emissivity of potential structural materials for very high temperature reactor systems: Hastelloy X, *Nucl. Technol.* 172 (2010) 88-100.
- [4] R.K. Maynard, N.M. Mokgalapa, T.K. Ghosh, R.V. Tompson, D.S. Viswanath, S.K. Loyalka, Hemispherical total emissivity of potential structural materials for very high temperature reactor systems: Haynes 230, *Nucl. Technol.* 179 (2012) 429-438.
- [5] L. Marchetti, S. Perrin, Y. Wouters, F. Martin, M. Pijolat, Photoelectrochemical study of nickel base alloys oxide films formed at high temperature and high pressure water, *Electrochem. Acta* 55 (2010) 5398-5392.
- [6] D. Kim, C. Jang, W.S. Ryu, Oxidation characteristics and oxide layer evolution of alloy 617 and Haynes 230 at 900°C and 1100°C, *Oxid. Metals* 71 (2009) 271-293.
- [7] B. Kong, T. Li, Q. Eri, Normal spectral emissivity of GH536 (Hastelloy X) in three surface conditions, *Appl. Thermal Eng.* 113 (2017) 20-26.
- [8] X. Ledoux, S. Mathieu, M. Vilasi, Y. Wouters, P. del Gallo, M. Wagner, Oxide growth characterization during short-time oxidation of a commercially available chromia-forming alloy (HR-120) in air at 1050°C, *Oxid. Metals* 80 (2013) 25-35.
- [9] B.V. Cockeram, D.P. Measures, A.J. Mueller, The development and testing of emissivity enhancement coatings for thermophotovoltaic (TPV) radiator applications, *Thin Solid Films* 355-356 (1999) 17-25.
- [10] M. Balat-Pichelin, J.F. Robert, J.L. Sans, Emissivity measurements on carbon-carbon composites at high temperature under high vacuum, *Appl. Surf. Sci.* 253 (2006) 778-783.

- [11] E. Brodu, M. Balat-Pichelin, J.L. Sans, J.C. Kasper, Influence of roughness and composition on the total emissivity of tungsten, rhenium and tungsten-25% rhenium alloy at high temperature, *J. Alloys Compds* 585 (2014) 510-517.
- [12] E. Brodu, M. Balat-Pichelin, J.L. Sans, M.D. Freeman, J.C. Kasper, Efficiency and behavior of textured high emissivity metallic coatings at high temperature, *Mater. Design* 83 (2015) 85-94.
- [13] D. Hernandez, J.L. Sans, A. Netchaieff, P. Ridoux, V. Le Sant, Experimental validation of a pyroreflectometric method to determine the true temperature on opaque surface without hampering reflections, *Measurement* 42 (2009) 836-843.
- [14] M. Balat-Pichelin, J.L. Sans, E. Bêche, V. Flaud, J. Annaloro, Oxidation and emissivity of Inconel 718 alloy as potential space debris during its atmospheric entry, *Mater. Charact.* 127 (2017) 379-390.
- [15] L. Barka, M. Balat-Pichelin, J.L. Sans, E. Bêche, Oxidation and emissivity of Invar 36 alloy in air plasma at high temperatures, *J. Alloys Compds* 772 (2019) 1003-1016.
- [16] H. Jo, J.L. King, K. Blomstrand, K. Sridgaran, Spectral emissivity of oxidized and roughened metal surfaces, *Int. J. Heat Mass Transfer* 115 (2017) 1065-1071.